Hindawi Publishing Corporation
International Journal of Antennas and Propagation
Volume 2014, Article ID 675036, 8 pages
http://dx.doi.org/10.1155/2014/675036

Research Article

Simple and Efficient Computational Method to Analyze Cylindrical Plasmonic Nanoantennas

Karlo Costa and Victor Dmitriev

Department of Electrical Engineering, Federal University of Para, Avenida Augusto Corrêa No 01, 66075-900 Belém, PA, Brazil

Correspondence should be addressed to Karlo Costa; karlo@ufpa.br

Received 24 November 2013; Revised 23 January 2014; Accepted 27 January 2014; Published 10 April 2014

Academic Editor: Michele Midrio

We present in this work a simple and efficient technique to analyze cylindrical plasmonic nanoantennas. In this method, we take into account only longitudinal current inside cylindrical structures and use 1D integral equation for the electric field with a given surface impedance of metal. The solution of this integral equation is obtained by the Method of Moments with sinusoidal basis functions. Some examples of calculations of nanoantennas with different geometries and sources are presented and compared with the commercial software Comsol 3D simulations. The results show that the proposed technique provides a good precision in the near-infrared and lower optical frequencies 100–400 THz.

1. Introduction

Optical antennas are metal nanostructures used to transmit or receive optical fields [1]. This definition is similar to that of conventional radio frequency (RF) and microwave antennas. The principal difference between these two regimes (RF microwave and optical one) is stipulated by the physical properties of the metals at optical frequencies. At these frequencies the metals cannot be considered as perfect conductors because of plasmonic effects [2]. Comprehensive reviews on optical antennas have been published in [3–6]. In these works, the authors presented recent developments, antenna parameters, applications, challenges, and future trends.

Conventional 3D techniques, for example, Green's tensor method [7, 8], the finite difference time domain method (FDTD) [9], the discrete dipole approximation (DDA) [10], and professional software, such as Comsol [11] and CST [12], have been used to analyze optical antennas. In general, all these techniques require high computational cost to make a precise analysis. Recently, simplified and efficient methods have been developed for analysis of cylindrical plasmonic nanoantennas [13–20]. These methods reduce the original 3D problem to 1D integral equation and provide much smaller computational cost in comparison with 3D techniques.

The first application of the surface impedance integral equation (SI-IE) for analysis of cylindrical optical antennas was presented in [13]. In this paper the authors solved the Hallén SI-IE for the finite-length dipole by Method of Moments (MoM), where they used a magnetic frill source, rectangular pulse function expansion, and point testing in the numerical solution. In [14, 15] the authors analyzed optical dipoles in the excitation mode by an incident plane wave and in the transmitting mode by a delta-gap source, where the MoM was used to solve numerically the Pocklington SI-IE to find the approximated linear current distribution. This same method was also used to analyze cylindrical optical antennas in uniaxial anisotropic media for tuning and control the optical response of the antenna [16]. V-shaped optical antennas have been analyzed in the wire approximation and SI-IE in [17]; in this case the authors used the Pocklington equation and the MoM with the Dirac basis functions. Other variations of the SI-IE method with Pocklington and Hallén equation can be found in [18, 19].

In [20] the SI-IE was obtained by the electric field integral equation (EFIE) with potential functions. In this paper the authors used the linear current approximation but they considered both the longitudinal and transversal current. These currents were approximated by a sinusoidal

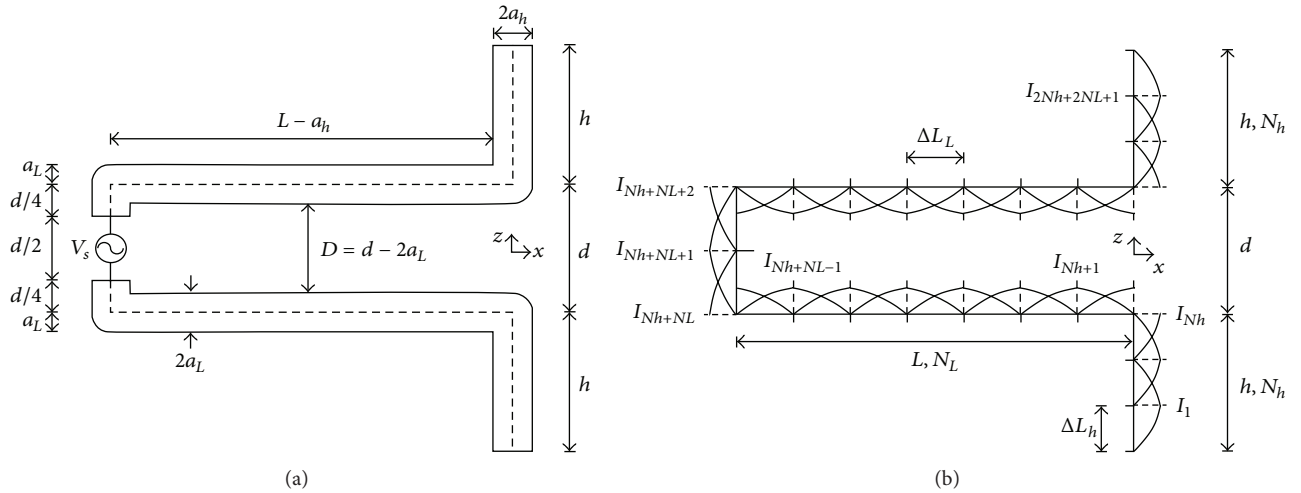

Figure 1: Cylindrical plasmonic nanocircuit composed of voltage source, optical transmission line, and nanodipole. (a) Geometry of the problem. (b) Discretization used in MoM model.

basis function expansion. Green's functions for these currents were obtained by numerical integration and closed form equations. The obtained results are in excellent agreement with 3D formulation up to 500 THz.

In this work, we present an efficient and simple alternative technique to analyze metallic cylindrical nanoantennas. The method is a simplified version of that presented in [20], because here we consider only longitudinal linear current inside the antenna; that is, we do not take into account transversal currents and use 1D integral equation for electric field with a given surface impedance of metal. The solution of this integral equation is obtained by linear Method of Moments (MoM) with sinusoidal basis functions, which provides solutions in closed form for the radiated electric fields from each current element. Some numerical examples of calculations of nanoantennas with different geometries and excitation sources are presented and compared with 3D methods. These results show that the proposed method provides a good efficiency in terms of precision and processing time when compared with more general 3D techniques approximately up to 400 THz.

2. Description of the Method

The method is based on the linear Method of Moments (MoM) with sinusoidal basis functions [21] and the equivalent surface impedance model [13]. The main ideas of the proposed method will be presented using a particular example of an optical nanocircuit composed of plasmonic cylindrical elements made of gold (Au) as shown in Figure 1. This circuit can be useful in nanophotonics to convert guided plasmonic optical waves in radiated field and vice versa and to make the input impedance matching between optical antennas and plasmonic waveguides [22, 23].

2.1. Integral Equation for Electric Field. Figure 1(a) shows an equivalent model of the antenna composed of a voltage source V_s, a two-wire optical transmission line (OTL), and a cylindrical nanodipole, and Figure 1(b) presents the MoM equivalent model. The dimensions of this nanocircuit are as follows: L and a_L are the length and radius of the OTL wires, respectively; $H = h + a_L$ and a_h are the arm length and radius of the nanodipole, respectively; d is the distance between the axes of the OTL; $D = d - 2a_L$ is the dipole gap and the distance between the surfaces of the OTL.

In the radiation problem of Figure 1(a), the gold material of the structure is represented by the Lorentz-Drude model for the complex permittivity $\varepsilon_1 = \varepsilon_0 \varepsilon_{r1}$ [24]:

$$\varepsilon_{r1} = \varepsilon_\infty - \frac{\omega_{p1}^2}{\omega^2 - j\Gamma\omega} + \frac{\omega_{p2}^2}{\omega_0^2 - \omega^2 + j\gamma\omega}, \tag{1}$$

where $\varepsilon_\infty = 8$, $\omega_{p1} = 13.8 \times 10^{15}\,\mathrm{s}^{-1}$, $\Gamma = 1.075 \times 10^{14}\,\mathrm{s}^{-1}$, $\omega_0 = 2\pi c/\lambda_0$, $\lambda_0 = 450\,\mathrm{nm}$, $\omega_{p2} = 45 \times 10^{14}\,\mathrm{s}^{-1}$, and $\gamma = 9 \times 10^{14}\,\mathrm{s}^{-1}$. This model is a good approximation with experimental data for wavelengths $\lambda > 500\,\mathrm{nm}$. The losses in metal are described by the surface impedance Z_s which is derived considering only the principal mode TM_{01} of infinite long cylindrical imperfect conductor [13]. In this case, the impedance is given by

$$Z_s = \frac{TJ_0(Ta)}{2\pi a j\omega\varepsilon_1 J_1(Ta)}, \tag{2}$$

where $T = k_0\sqrt{\varepsilon_{r1}}$, $k_0 = \omega\sqrt{\mu_0\varepsilon_0}$, and J_0 and J_1 are the zeroth- and first-order Bessel functions of the first kind, respectively.

The boundary condition for the electric field at the surface's conductor of the circuit in Figure 1(a) is $(\overline{E}_s + \overline{E}_i) \cdot \overline{a}_l = Z_s I$, where $\overline{a}_l$ is the unitary vector tangential to the surface of the metal, $\overline{E}_s$ is the scattered electric field due to the induced linear current I (A) on the conductor, $\overline{E}_i$ is the incident electric field from the voltage source, and I is the longitudinal current in a given point of the nanocircuit. The

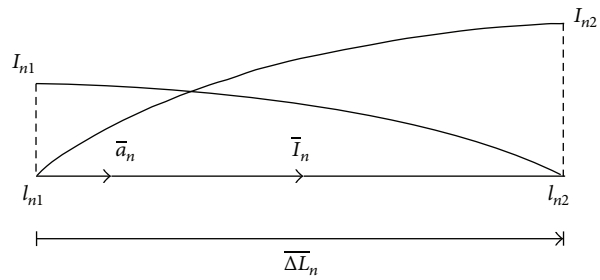

Figure 2: Sinusoidal current element in one segment.

integral equation of the scattered field along the length l of the nanocircuit is

$$\overline{E}_s(\overline{r}) = \frac{1}{j\omega\varepsilon_0}\left[k_0^2\int_l \overline{I}g(R)\,dl' + \int_l \frac{dI}{dl'}\nabla g(R)\,dl'\right], \quad (3)$$

where $g(R) = e^{-jk_0R}/4\pi R$ is the free space Green's function and $R = |\overline{r}-\overline{r}'|$ is the distance between source and observation points.

2.2. Numerical Solution by Method of Moments. Numerical solution of the problem formulated by (1)–(3) is performed by linear MoM as follows. Firstly, we discretize the linear circuit as shown in Figure 1(b), where N_L and N_h are the number of straight segments in L and h, respectively. In the case shown in Figure 1(b), we have $N_L = 7$ and $N_h = 3$. The discretization is uniform in L and h, but the discretization length can be different; that is, $\Delta L_L = L/N_L$ and $\Delta L_h = h/N_h$. The voltage source gap is $d/2$, and there are two segments in vertical section of this source. With this discretization, the total number of straight segments of the nanocircuit is $N = 2N_h + 2N_L + 2$. Now, the current in each segment is approximated by sinusoidal basis functions as follows:

$$i_n = \frac{1}{\sinh\gamma\Delta l_n}\left[I_{n1}\sinh\gamma(l_{n2}-l) + I_{n2}\sinh\gamma(l-l_{n1})\right],$$

$$\gamma = jk_0,$$

$$\overline{I} = \sum_{n=1}^{N}\overline{I}_n = \sum_{n=1}^{N} i_n\overline{a}_n, \quad (4)$$

where $\overline{a}_n$ is the unitary vector tangential to the axis of each cylindrical metallic element (Figure 2).

Substituting (4) in (3), we obtain the discrete form of the integral equation:

$$\overline{E}_s = \sum_{n=1}^{N}\left[L\overline{I}_n\right],$$

$$L\overline{I}_n = \frac{1}{j\omega\varepsilon_0}\left(-\gamma^2\int_{l_{n1}}^{l_{n2}}\overline{I}_n\left(l'\right)g(R)\,dl' + \int_{l_{n1}}^{l_{n2}}\frac{dI_n}{dl'}\nabla g(R)\,dl'\right). \quad (5)$$

A generic sinusoidal element is presented in Figure 2. Each sinusoidal current element can be written in the form

$$\overline{I}_n = I_{n1}\overline{f}_{n1} + I_{n2}\overline{f}_{n2},$$
$$\overline{f}_{n1} = \frac{\sinh\gamma(l_{n2}-l)}{\sinh\gamma\Delta l_n}\overline{a}_n, \qquad \overline{f}_{n2} = \frac{\sinh\gamma(l-l_{n1})}{\sinh\gamma\Delta l_n}\overline{a}_n. \quad (6)$$

Substituting (6) and (5) in the boundary condition for the electric field and using the conditions $I_{12} = I_{21} = I_1, \ldots, I_{n2} = I_{(n+1)1} = I_n, \ldots, I_{(N-1)2} = I_{N1} = I_{(N-1)}$, and $I_{11} = I_{N2} = 0$ at the extremities of the conductor, we have

$$\left[\overline{E}_i\cdot\overline{a}_l + \sum_{n=1}^{N-1}\left(L\overline{f}_{n2} + L\overline{f}_{(n+1)1}\right)I_n\cdot\overline{a}_l\right] = Z_sI. \quad (7)$$

The expansion constants I_n are shown in Figure 1(b), where each constant I_n defines one triangular sinusoidal current. To determine these constants, we use $N-1$ rectangular pulse test functions with the unit amplitude

$$P_m(l) = \begin{cases}1, & l_{mc} < l < l_{(m+1)c},\\ 0, & \text{outside},\end{cases}$$
$$m = 1, 2, 3, \ldots, N-1, \quad (8)$$

where l_{mc} is the middle point between l_{m1} and l_{m2} of each segment m (Figure 2). Integrating both sides of (7) with a generic test function P_m of (8), we come to the following equation:

$$\left[\int_{l_{mc}}^{l_{(m+1)c}}\overline{E}_i\cdot\overline{a}_l dl + \int_{l_{mc}}^{l_{(m+1)c}}\sum_{n=1}^{N-1}\left(L\overline{f}_{n2} + L\overline{f}_{(n+1)1}\right)I_n\cdot\overline{a}_l dl\right] = \int_{l_{mc}}^{l_{(m+1)c}} Z_sI\,dl. \quad (9)$$

For $m = 1, 2, 3, \ldots, N-1$, we have the following linear system:

$$V_m = Z_sI_m\Delta_m - \sum_{n=1}^{N-1}Z_{mn}I_n, \quad m = 1, 2, 3, \ldots, N-1,$$
$$Z_{mn} = \int_{l_{mc}}^{l_{(m+1)c}}\left[L\overline{f}_{n2} + L\overline{f}_{(n+1)1}\right]\cdot\overline{a}_l dl, \quad (10)$$
$$V_m = \int_{l_{mc}}^{l_{(m+1)c}}\overline{E}_i\cdot\overline{a}_l dl, \qquad \int_{l_{mc}}^{l_{(m+1)c}} Z_sI\,dl = Z_sI_m\Delta_m,$$

where $\Delta_m = 1/2[\Delta L_m + \Delta L_{m+1}]$, V_m is the equivalent voltage in each segment m; V_m is nonzero only in the position of the voltage source in $m = N/2$ with value $V_{N/2} = V_s$. In this case we have a radiation problem. When V_m is due to an incident radiation, which can be, for example, a plane wave, we have a scattering problem. Z_{mn} is the mutual impedance between sinusoidal current elements m and n. In matrix form, the following system of the order $(N-1)\times(N-1)$ is obtained:

$$\begin{bmatrix} -Z_{11}+Z_s\Delta_1 & -Z_{12} & \cdots & -Z_{1(N-1)} \\ -Z_{21} & -Z_{22}+Z_s\Delta_2 & \cdots & -Z_{2(N-1)} \\ \vdots & \vdots & \ddots & \vdots \\ -Z_{(N-1)1} & -Z_{(N-1)2} & \cdots & -Z_{(N-1)(N-1)}+Z_s\Delta_{(N-1)} \end{bmatrix} \begin{bmatrix} I_1 \\ I_2 \\ \vdots \\ I_{N-1} \end{bmatrix} = \begin{bmatrix} V_1 \\ V_2 \\ \vdots \\ V_{N-1} \end{bmatrix}. \tag{11}$$

To calculate the elements Z_{mn} of this linear system one needs to solve the integral of (5). Approximated closed form solutions of (5) for the electric fields produced by one sinusoidal current segment of (6) can be found in the literature [21]. To calculate the electric fields in the local coordinate system of Figure 3, we used the following analytical expressions:

$$E_l = \frac{\eta}{4\pi \sinh \gamma\Delta L_n}\left[\left(I_{n1} - I_{n2}\cosh\gamma\Delta L_n\right)\frac{e^{-\gamma R_2}}{R_2} + \left(I_{n2} - I_{n1}\cosh\gamma\Delta L_n\right)\frac{e^{-\gamma R_1}}{R_1}\right],$$

$$E_\rho = \frac{\eta}{4\pi\rho \sinh \gamma\Delta L_n}\left\{\left(I_{n1}e^{-\gamma R_1} - I_{n2}e^{-\gamma R_2}\right)\sinh\gamma\Delta L_n + \left(I_{n1}\cosh\gamma\Delta L_n - I_{n2}\right)\cos\theta_1 e^{-\gamma R_1} + \left(I_{n2}\cosh\gamma\Delta L_n - I_{n1}\right)\cos\theta_2 e^{-\gamma R_2}\right\}. \tag{12}$$

The solution of (11) produces the induced current I_n along the circuit. With this solution, it is possible to calculate the near and far field distributions of the electric field and other parameters.

3. Numerical Results

Based on the theory presented in the previous section, we developed a MoM code in Matlab to analyze the nanocircuit shown in Figure 1. The simulations were performed in a core i7 computer with 4 G of RAM in Windows. Some simulations were also realized with the software Comsol in a core i7 computer with 16 G of RAM. It is important to note here that all of our simulations with the MoM code were finalized approximately within 2 min, but the simulation by the Comsol after 4 hours.

3.1. Resonances of Nanorods Excited by Plane Wave. The developed MoM code can be used to analyze the near field resonances of nanorods excited by a plane wave. To this end, we modify only the geometry and the source of the original problem (Figure 1). Examples of plane wave excitation of nanorods are presented in Figure 4. This figure shows the spectral response of the normalized electric near field $|E|/|E_0|$ (where $|E|$ is the magnitude of the total electric near field and $|E_0|$ is the electric field magnitude of the incident plane wave) in the point P near the endpoint of a single nanorod and in the middle between the two nanorods. The parameters used in these simulations are as follows: $H = h + a_L = 220$ nm, $a_h = 10$ nm, $D = 20$ nm, $N_h = 11$, and $\Delta L_h = 20$ nm. With this discretization we have a good agreement with the Comsol results and the convergence criteria $\min(\Delta L_h)/a_h \geq 1$ that we used are satisfied. In the discussed case, we have $\min(\Delta L_h)/a_h = 2$.

For the case of the single nanorod in Figure 4, the main resonances calculated by MoM and by Comsol are $F_{\text{res}} = 235.7$ THz ($\lambda_{\text{res}} = 1273$ nm) and $F_{\text{res}} = 235$ THz ($\lambda_{\text{res}} = 1277$ nm), respectively. Therefore, a good agreement between the results obtained by the two methods is observed. We have also calculated the variation of the main resonant wavelength (λ_{res}) of one nanorod with different lengths $H = h + a_h$ and radius a_h. The consistent results obtained by MoM, Comsol and data obtained in [25] are presented in Figure 5. These results are in accordance with the scaling rule of the effective wavelength for cylindrical optical antennas [26]. For RF microwave dipoles, the linear dependence of λ_{res} with length H is $\lambda_{\text{res}} = 2H$, but for the nanorods in Figure 4, we have the approximated linear dependence of $\Delta\lambda_{\text{res}}/\Delta H \approx 6.8$, $\Delta\lambda_{\text{res}}/\Delta H \approx 4$, and $\Delta\lambda_{\text{res}}/\Delta H \approx 2.6$ for the radius $a_h = 5, 10$, and 20 nm, respectively. This means that the smaller radius corresponds to higher inclination of the curves or higher resonant wavelengths. These results show also that nanorods are electrically smaller than conventional metallic rods in RF microwave with $\lambda/2$ resonance.

3.2. Input Impedance. Figures 6 and 7 show the input impedances of two circuits of Figure 1 with $L = 0$ and 100 nm, respectively. The dimensions $H = h + a_L = 220$ nm, $a_L = a_h = 10$ nm, and $D = 20$ nm are fixed for both circuits. The simulation parameters used in MoM and Comsol methods are presented in the figure captions. In the MoM simulations, we use the convergence criteria $\min(\Delta L_L/a_L) \geq 2$ and $\min(\Delta L_h/a_h) \geq 2$.

The results presented in these figures show a good agreement between the two methods. However, the MoM method results in smaller computational costs in terms of required memory and processing time. In the MoM model, one uses 1D current elements approximation for cylindrical conductors instead of 3D current elements inside the conductor in Comsol simulations. Also, the MoM discretizes only the conductors, and the Comsol discretizes the conductors and the domain around the conductors. This is why the MoM model requires a reduced number of unknown elements in the entire problem and, consequently, reduced memory and processing time in comparison with the Comsol simulation. For example, in Figure 7 we used $N = 32$ elements for MoM with the processing time of 15 seconds and for Comsol we used 622327 elements with the processing time of 5 hours.

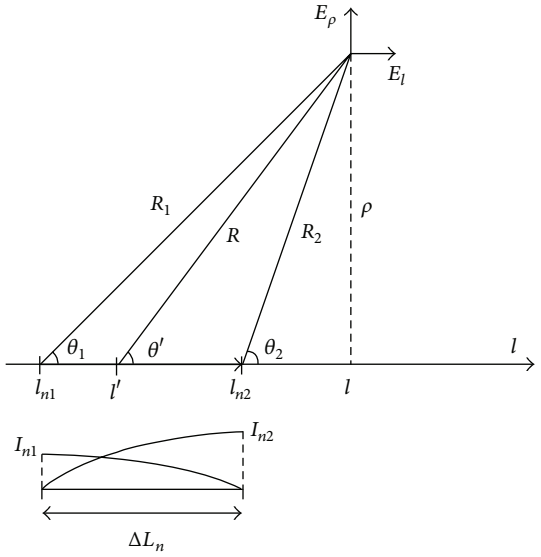

FIGURE 3: Local coordinate system of one generic sinusoidal current segment of (6) used for calculation of components of radiated electric fields in (12).

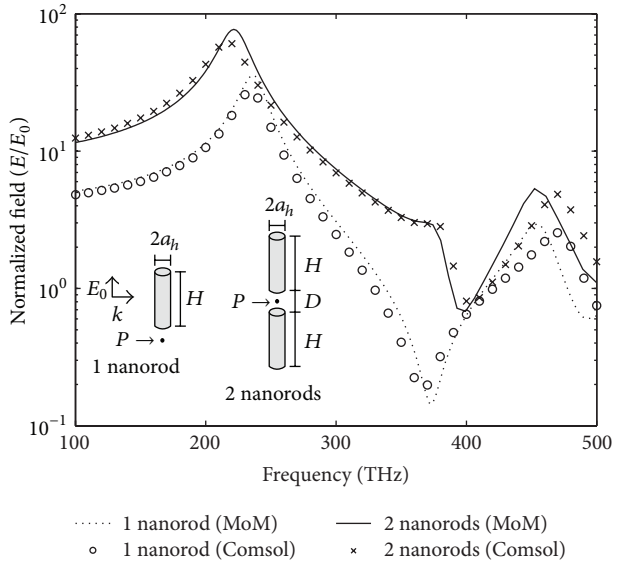

FIGURE 4: Normalized electric field near single and two nanorods at point P (10 nm from the nanorods edge), incident plane wave with amplitude E_0. The nanorods are made of Au, $N = 11$, $H = 220$ nm, $a_h = 10$ nm, and $d = 20$ nm.

In both methods (MoM and Comsol), we have carried out all the simulations in 3D surroundings. In the MoM model, we do not need radiation boundary condition because this method already takes into account this condition in the free space Green's function. In the Comsol method, we used a spherical domain with PLM in the external boundary to simulate the free space and the lumped port source to simulate a voltage source.

3.3. Impedance Matching Characteristics of Nanocircuit. This section presents an example of impedance matching analysis

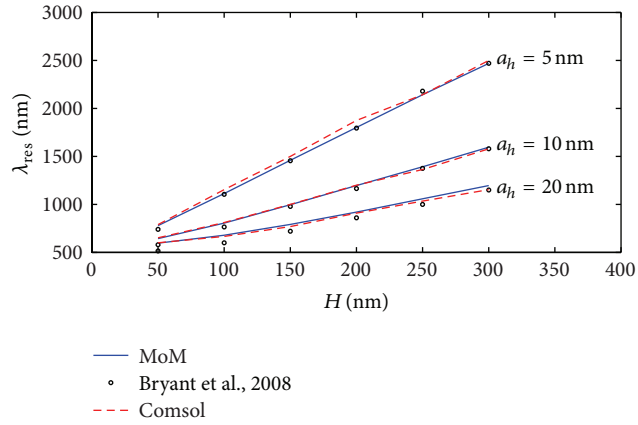

FIGURE 5: Resonant wavelength of $\lambda/2$ mode versus length H for different values of radius a_h.

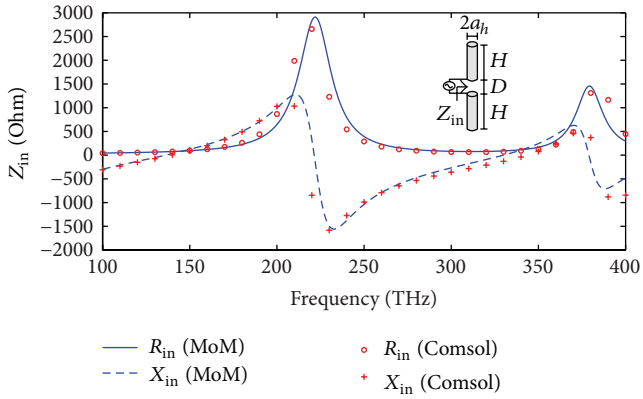

FIGURE 6: Input impedance of isolated nanodipole with $L = 0$ nm, $H = h + a_L = 220$ nm, $a_L = a_h = 10$ nm, and $D = 20$ nm. Parameters of MoM simulation are number of elements: $N = 24$, processing time: 10 sec. Parameters of the Comsol simulation are number of elements: 376629, minimum element mesh size of the conductors: 0.408 nm, minimum element mesh size of the spherical domain: 8.16 nm, and processing time: 2 h 34 min.

of the nanocircuit shown in Figure 1(a). In this example, we used the following parameters: $h = 210$ nm, $L = 1200$ nm, $a_L = a_h = 10$ nm, $d = 40$ nm, $N_h = 10$, $N_L = 40$, $\Delta L_L = 30$ nm, $\Delta L_h = 21$ nm, and $N = 102$. The discretization in the vertical section of the source is $\Delta L = 20$ nm. With these values, the convergence criteria are satisfied, that is, $\min(\Delta L/a) \geq 2$. Figure 8 shows the dimensions and sizes of the discretization. The corners of the circuit are numbered from 1 to 4.

To make a quantitative measure of the impedance matching, we calculate approximately the voltage stationary wave ratio (VSWR) near the dipole as VSWR $= I_{max}/I_{min}$, where I_{max} and I_{min} are, respectively, the maximum and minimum current magnitudes nearest to the dipole. With this parameter, we calculate approximately the voltage reflection coefficient as $|\Gamma_V| = (\text{VSWR} - 1)/(\text{VSWR} + 1)$. Figure 9 shows the variation of $|\Gamma_V|$ versus frequency. In this figure, the minimum value of the reflection coefficient is

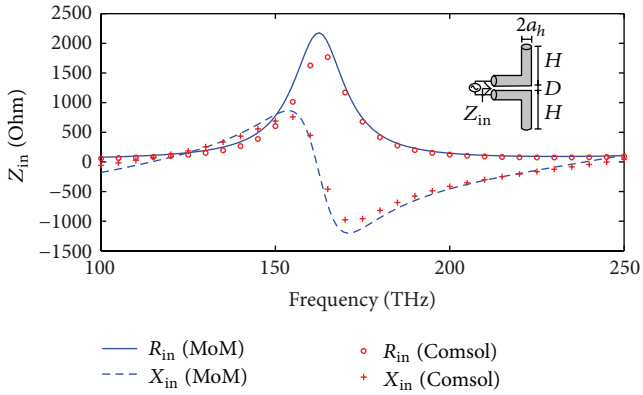

FIGURE 7: Input impedance of nanocircuit with $L = 100$ nm, $H = h + a_L = 220$ nm, $a_L = a_h = 10$ nm, and $D = 20$ nm. Parameters of the MoM simulation are number of elements: $N = 32$, processing time: 15 sec. Parameters of Comsol simulation are number of elements: 622327, minimum element mesh size of conductors: 0.3 nm, minimum element mesh size of spherical domain: 32.4 nm, and processing time: 5 h.

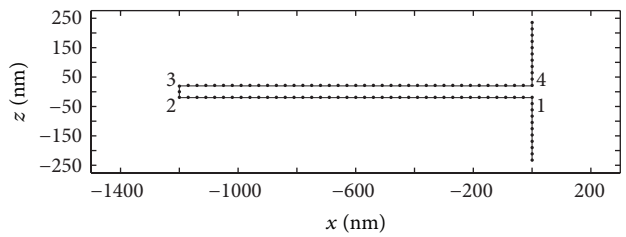

FIGURE 8: Discretization of simulated nanocircuit. Parameters are $h = 210$ nm, $L = 1200$ nm, $a_L = a_h = 10$ nm, $d = 40$ nm, $N_h = 10$, $N_L = 40$, $\Delta L_L = 30$ nm, $\Delta L_h = 21$ nm, and $N = 102$.

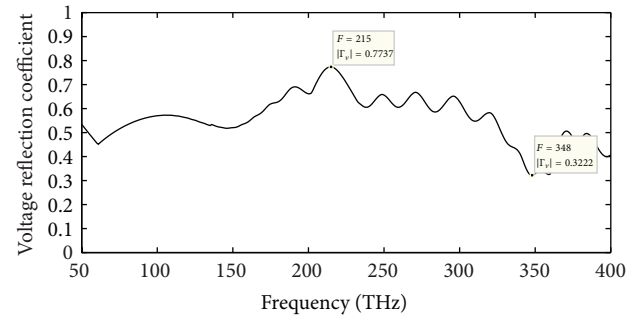

FIGURE 9: Voltage reflection coefficient $|\Gamma_V|$ near dipole of nanocircuit with parameters $h = 210$ nm, $L = 1200$ nm, $a_L = 10$ nm, $a_h = 10$ nm, $d = 40$ nm, $N_h = 10$, $N_L = 40$, $\Delta L_L = 30$ nm, $\Delta L_h = 21$ nm, and $N = 102$.

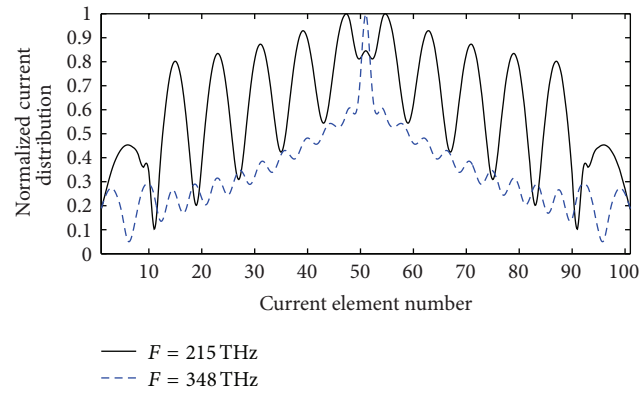

FIGURE 10: Current distributions along nanocircuit at frequencies $F = 215$ and 348 THz for cases with voltage reflection coefficient $|\Gamma_V| = 0.77$ and 0.32, respectively. Parameters of MoM simulation are $h = 210$ nm, $L = 1200$ nm, $a_L = a_h = 10$ nm, $d = 40$ nm, $N_h = 10$, $N_L = 40$, $\Delta L_L = 30$ nm, $\Delta L_h = 21$ nm, and $N = 102$.

$|\Gamma_V| = 0.32$ at $F = 348$ THz, and the maximum value of the reflection coefficient is $|\Gamma_V| = 0.77$ at $F = 215$ THz. The current distribution and the normalized electric field in these two different situations are presented in Figures 10 and 11, respectively. These results show that our approximate method to calculate $|\Gamma_V|$ gives a good estimate of degree of impedance matching.

The input impedance of the isolated nanodipole versus frequency presented in Figure 6 at the points $|\Gamma_V| = 0.77$ and 0.32 is $Z_{in} = 2148 + j1116$ (Ω) and $Z_{in} = 155.4 + j219.1$ (Ω), respectively. The first impedance is near the first open-circuit resonance, and the second impedance is near the second short-circuit resonance of the nanodipole. These types of resonances can be observed in Figure 10.

4. Conclusions

We presented a simple and efficient computational method to analyze cylindrical plasmonic nanoantennas. We described details of the method which is based on the linear Method of Moments with sinusoidal basis functions. The losses in the conductors were taken into account by equivalent surface impedance. Some examples of nanoantenna were simulated and compared with the results obtained by the Comsol software. These examples include nanorods illuminated by an incident plane wave, nanodipoles fed by a voltage source, and a nanocircuit composed of a voltage source, a two-wire optical transmission line, and a nanodipole.

Our results show that the proposed method is computationally simple and produces results with a good agreement with the Comsol simulations up to lower optical frequencies ($F \approx 400$ THz). For higher frequencies, in general, the method is not valid, because transversal current in the cylindrical conductors will appear and in our method only longitudinal currents are taken into account. Thus, the method is suitable for near-infrared and lower optical frequencies (100–400) THz. With respect to the time processing, the proposed method is very fast when compared with the Comsol simulations. For example, the results presented in Figure 4 were obtained by the Method of Moments within 1 min, but the corresponding calculations by the software Comsol were accomplished within 4 hours.

In future works we intend to modify our method to take into account transversal currents in the cylindrical conductors. It will allow one to apply the method at higher

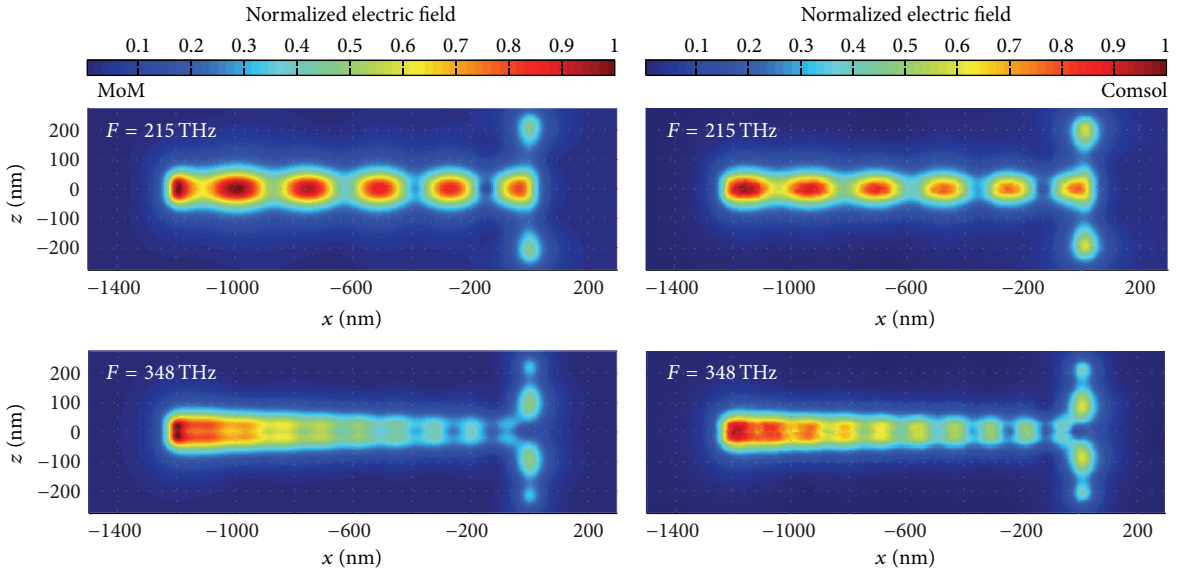

Figure 11: Normalized electric near field distributions at plane $y = 40$ nm of nanocircuit at frequencies $F = 215$ and 348 THz for cases with voltage reflection coefficient $|\Gamma_V| = 0.77$ and 0.32, respectively. Parameters of MoM simulation are $h = 210$ nm, $L = 1200$ nm, $a_L = a_h = 10$ nm, $d = 40$ nm, $N_h = 10$, $N_L = 40$, $\Delta L_L = 30$ nm, $\Delta L_h = 21$ nm, $N = 102$, and processing time 3 min. Parameters of Comsol simulation are total number of elements: 713095, minimum mesh size of the conductors: 2.55 nm, minimum mesh size of spherical domain: 30.6 nm, and processing time: 5 hours.

optical frequencies. Also, the method can be used for analysis and design of nanoantenna systems, composed of cylindrical elements, for example, arrays of nanodipoles. Also, the method can be used to make the input impedance matching of nanodipoles with optical transmission line in order to optimize the energy transfer from source to load.

Conflict of Interests

The authors declare that there is no conflict of interests regarding the publication of this paper.

Acknowledgments

This work was supported by the Brazilian agencies PROPESP/UFPA and FADESP.

References

[1] P. Bharadwaj, B. Deutsch, and L. Novotny, "Optical antennas," *Advances in Optics and Photonics*, vol. 1, pp. 438–483, 2009.

[2] S. A. Maier, *Plasmonics: Fundamentals and Applications*, Springer, 2007.

[3] L. Novotny and N. van Hulst, "Antennas for light," *Nature Photonics*, vol. 5, no. 2, pp. 83–90, 2011.

[4] P. Biagioni, J.-S. Huang, and B. Hecht, "Nanoantennas for visible and infrared radiation," *Reports on Progress in Physics*, vol. 75, no. 2, Article ID 024402, 2012.

[5] A. Alù and N. Engheta, "Theory, modeling and features of optical nanoantennas," *IEEE Transactions on Antennas & Propagation*, vol. 61, no. 4, pp. 1508–1517, 2013.

[6] V. Giannini, A. I. Fernández-Domínguez, S. C. Heck, and S. A. Maier, "Plasmonic nanoantennas: fundamentals and their use in controlling the radiative properties of nanoemitters," *Chemical Reviews*, vol. 111, no. 6, pp. 3888–3912, 2011.

[7] K. Q. Costa and V. A. Dmitriev, "Analysis of modified bowtie nanoantennas in the excitation and emission regimes," *Progress in Electromagnetics Research B*, no. 32, pp. 57–73, 2011.

[8] F. P. G. de Arquer, V. Volski, N. Verellen, G. A. E. Vandenbosch, and V. V. Moshchalkov, "Engineering the input impedance of optical nano dipole antennas: materials, geometry and excitation effect," *IEEE Transactions on Antennas and Propagation*, vol. 59, no. 9, pp. 3144–3153, 2011.

[9] Z. L. Yang, Q. H. Li, F. X. Ruan et al., "FDTD for plasmonics: applications in enhanced Raman spectroscopy," *Chinese Science Bulletin*, vol. 55, no. 24, pp. 2635–2642, 2010.

[10] B. T. Draine and P. J. Flatau, "Discrete-dipole approximation for scattering calculations," *Journal of the Optical Society of America A*, vol. 11, no. 4, pp. 1491–1499, 1994.

[11] COMSOL Multiphysics 4.2a, COMSOL Inc.http://www.comsol.com/.

[12] CST-Microwave-Studio, http://www.cst.com/.

[13] G. W. Hanson, "On the applicability of the surface impedance integral equation for optical and near infrared copper dipole antennas," *IEEE Transactions on Antennas and Propagation*, vol. 54, no. 12, pp. 3677–3685, 2006.

[14] A. Locatelli, C. de Angelis, D. Modotto et al., "Modeling of enhanced field confinement and scattering by optical wire antennas," *Optics Express*, vol. 17, no. 19, pp. 16792–16800, 2009.

[15] C. de Angelis, A. Locatelli, D. Modotto et al., "Extending antenna theory to the optical domain," in *Proceedings of the 39th European Microwave Conference (EuMC '09)*, pp. 810–813, October 2009.

[16] C. de Angelis, A. Locatelli, D. Modotto, S. Boscolo, M. Midrio, and A.-D. Capobianco, "Frequency addressing of nano-objects

by electrical tuning of optical antennas," *Journal of the Optical Society of America B*, vol. 27, no. 5, pp. 997–1001, 2010.

[17] R. Blanchard, G. Aoust, P. Genevet et al., "Modeling nanoscale V-shaped antennas for the design of optical phased arrays," *Physical Review B*, vol. 85, no. 15, Article ID 155457, 2012.

[18] A. M. A. Sabaawi, C. C. Tsimenidis, and B. S. Sharif, "Analysis and modeling of infrared solar rectennas," *IEEE Journal of Selected Topics in Quantum Electronics*, vol. 19, no. 3, Article ID 9000208, 2013.

[19] C. Kremers and D. N. Chigrin, "Light scattering on nanowire antennas: a semi-analytical approach," *Photonics and Nanostructures*, vol. 9, no. 4, pp. 358–366, 2011.

[20] A. Rashidi, H. Mosallaei, and R. Mittra, "Scattering analysis of plasmonic nanorod antennas: a novel numerically efficient computational scheme utilizing macro basis functions," *Journal of Applied Physics*, vol. 109, no. 12, Article ID 123109, 2011.

[21] L. D. Grcev and F. E. Menter, "Transient electromagnetic fields near large earthing systems," *IEEE Transactions on Magnetics*, vol. 32, no. 3, pp. 1525–1528, 1996.

[22] J. Wen, S. Romanov, and U. Peschel, "Excitation of plasmonic gap waveguides by nanoantennas," *Optics Express*, vol. 17, no. 8, pp. 5925–5932, 2009.

[23] J.-S. Huang, T. Feichtner, P. Biagioni, and B. Hecht, "Impedance matching and emission properties of nanoantennas in an optical nanocircuit," *Nano Letters*, vol. 9, no. 5, pp. 1897–1902, 2009.

[24] L. Novotny and B. Hecht, *Principles of Nano-Optics*, Cambridge University Press, New York, NY, USA, 2006.

[25] G. W. Bryant, F. J. García de Abajo, and J. Aizpurua, "Mapping the plasmon resonances of metallic nanoantennas," *Nano Letters*, vol. 8, no. 2, pp. 631–636, 2008.

[26] L. Novotny, "Effective wavelength scaling for optical antennas," *Physical Review Letters*, vol. 98, no. 4, Article ID 266802, 2007.